J Nanopart Res (2016) 18: 338
DOI 10.1007/s11051-016-3642-4

RESEARCH PAPER

Facile and scalable fabrication engineering of fullerenol nanoparticles by improved alkaline-oxidation approach and its antioxidant potential in maize

Fu-yang Liu · Feng-xia Xiong · Yi-kang Fan · Juan Li · He-zhong Wang · Geng-mei Xing · Feng-ming Yan · Fu-ju Tai · Rui He

Received: 16 July 2016 / Accepted: 21 October 2016 / Published online: 16 November 2016

Abstract A feasible in operation, labor-saving and low-cost one-step technology to fabricate fullerenol nanoparticles (FNPs) up to 10 g in laboratory was developed by improved alkaline-oxidation approach using moderately concentrated sodium hydroxide solution as the hydroxylation agent and o-dichlorobenzene as the solvent. This strategy paves the avenue for industrial-scale bulk production of FNPs. The resulted product, $[C_{60}(OH)_{22}{\cdot}8H_2O]_n$, were characterized by various measurements including matrix-assisted laser desorption ionization time-of-flight mass spectrometry, high-resolution ^1H nuclear magnetic resonance spectrometry, Fourier transform infrared spectroscopy, UV-Visible spectrophotometer, thermogravimetric analysis, differential scanning calorimetry, dynamic light scattering analysis, scanning electron microscopy, and electron spin resonance spectrometer. Radical scavenging assay in vitro confirmed the high efficiency of water-soluble $[C_{60}(OH)_{22}{\cdot}8H_2O]_n$ as a novel radical scavenger. Furthermore, $[C_{60}(OH)_{22}{\cdot}8H_2O]_n$ as an excellent candidate has the potential to serve as the plant defense stimulation agent in maize.

Keywords Fullerenol · One-step · Scalable · Antioxidant · Maize · Carbon-based nanomaterials

Introduction

Fullerenols was the most promising water-soluble derivatives of fullerenes, which was known as nanoassembly into clusters in the form of fullerenol nanoparticles (FNPs) (Djordjevic et al. 2015; Wang et al. 2015b). FNPs as model carbon-based nanomaterials (CNMs) exhibited excellent capabilities in the quenching of various physiologically relevant free radicals compared to conventional antioxidants. The antioxidant properties and potential application in nanomedicine of FNPs have extracted extensive attentions in the past decades, which were described in the comprehensive review papers (Chen et al. 2012; Djordjevic et al. 2015; Grebowski et al. 2013; Markovic and Trajkovic 2008; Nielsen et al. 2008; Wang et al. 2015b). The successful and tremendous applications of FNPs in nanomedicine have also raised considerable concerns in agriculture. For example, the first report on FNPs enhancing plant biomass and fruit

Fu-yang Liu and Feng-xia Xiong contributed equally to this work.

F.-y. Liu · F.-j. Tai (✉)
Collaborative Innovation Center of Henan Grain Crops, State Key Laboratory of Wheat and Maize Crop Science, College of Life Science, Henan Agricultural University, Zhengzhou 450002, China
e-mail: taifj2008@163.com

F.-x. Xiong · Y.-k. Fan · H.-z. Wang · F.-m. Yan · R. He (✉)
NanoAgro Center, College of Plant Protection, Henan Agricultural University, 63 Nongye Road, Zhengzhou 450002, China
e-mail: herui@henau.edu.cn

J. Li · G.-m. Xing
Lab. for Bio-Environmental Health Sciences of Nanoscale Materials, Institute of High Energy Physics, Chinese Academy of Sciences, Beijing 100049, China

yield published in 2013, using bitter melon as a modal to evaluate the effects of $C_{60}(OH)_{20}$ FNPs on seeds (Kole et al. 2013). Gao et al. reported that $C_{60}(OH)_{24–26}$ FNPs stimulated seedling growth of *Arabdopsis thaliana* (Gao et al. 2011). The results revealed that FNPs have possible promises for applications on regulating plant growth and boosting crop production and quality in agriculture. To be agriculturally useful, the major problem to overcome stems from the small-scale productivity and intolerably high costs in FNPs production. Therefore, facilitating the economical mass production and decreasing costs become necessary for agricultural applications of FNPs.

Various synthesis methods of FNPs have extensively been investigated since the early 1990s, including the use of nitronium chemistry (Chiang et al. 1992b), sulfuric and nitric acid (Chiang et al. 1992a; Chiang et al. 1993; Vileno et al. 2006), hydroboration (Schneider et al. 1994), oleum (Chiang et al. 1994), radical reaction (Chiang et al. 1996; Ratnikova et al. 2004), potassium (Arrais and Diana 2003), solid-state mechanochemical reaction (Zhang et al. 2003), polybrominated derivative (Mirkov et al. 2004), solvent-free reaction (Wang et al. 2005), hydrogen peroxide (Kokubo et al. 2008; Kokubo et al. 2011), sodium zincate (Wang et al. 2010), alkaline-oxidation (Alves et al. 2006; Husebo et al. 2004; Li et al. 1993, 2012a; Xing et al. 2004; Yao et al. 2010; Zhang et al. 2004), and so on. Among these methods, one of the predominated pathways to fabricate FNPs is O_2/NaOH approach developed by Li et al. in 1993 (Li et al. 1993). This reaction was a few volume of extremely concentrated NaOH solution (e.g., 1.0 g/ml) with fullerene assisted by catalyst tetra-*n*-butylammonium hydroxide (TBAH) at room temperature under air atmosphere, followed by washing and precipitation with a huge amount of methanol and further purification. Henceforward, several research groups were dedicated to modify or improve this path, for example, using a large volume of extremely concentrated NaOH solution and prolonging reaction time from 10 h to 2 days (Husebo et al. 2004), adjusting the feed ratio of NaOH to fullerene (Xing et al. 2004), substituting of TBAH with PEG 400 (Alves et al. 2006; Zhang et al. 2004), replacing methanol precipitation by dialysis (Yao et al. 2010), as well as separation of the different components of FNPs with isoelectric focusing technology (Li et al. 2012a; Xiong et al. 2016). Furthermore, it was evidenced on the basis of experiments and calculations that oxygen (O_2) played an important role in these procedures (Alves et al. 2006; Husebo et al. 2004; Wang et al. 2015a; Wang et al. 2015b; Xing et al. 2004). Recently, the reasonable mechanism of FNP formation under O_2/NaOH condition has been studied by density functional theory calculations that the reaction experienced via three steps: hydroxylation, i.e., nucleophilic addition of OH^-; oxidation, i.e., electrophilic addition of O_2; and structural rearrangement (Wang et al. 2015a). Although being a currently popular and powerful method in laboratory from an academic point of view, facile and scalable fabrication of FNPs with O_2/NaOH still has several disadvantages from an engineering point of view. First is the uncontrollability and insufficient of the oxidation in laboratory practice and consequently the generation of a mass of water-insoluble by-product. Secondly, the resulted products, such as $C_{60}(OH)_x$ x = 8.5 (Zhang et al. 2004), x = 18–20 (Alves et al. 2006), x = 24–26 (Li et al. 1993), x = 27 (Zhang et al. 2004), x = 30, 32, 36, 42, 44 (Xing et al. 2004), or, $Na_n^+[C_{60}O_x(OH)_y]^{n-}$ n = 2–3, x = 7–9, y = 12–15 (Husebo et al. 2004), do not have good reproducibility due to their complicated structure and chemical composition, which have variable number and sites of hydroxyl groups (−OH) on the surface of the fullerene cages, and possibly, the simultaneous formation of impure groups such as ketone structures (Husebo et al. 2004; Xing et al. 2004). Thirdly, the solubility of fullerene in the reported solvents is very low at room temperature (i.e., the solubilities of C_{60} were 1.7 and 2.8 mg/mL in benzene and in toluene (Beeby et al. 1994), respectively) and also is a barrier to large-scale bulk production of FNPs. Finally, the consumption of extremely concentrated NaOH solution and a large amount of toluene (or benzene) and methanol is associated with strong corrosion and heavy pollution, and also is quite uneconomical.

Herein, we further improved the method to fabricate FNPs under O_2/NaOH condition up to super 10 g in laboratory, as a facile, labor-saving, economical, and efficient one-step technique using mildly concentrated NaOH solution (i.e., 0.1 g/mL) as the hydroxylation agent and the solvent with high-density and high dissolving capacity, followed by dialysis. That is, to our knowledge by far, the simplest one-step strategy of facile and large-scale fabrication of FNPs. The novel FNPs were characterized by various spectroscopic methods, the thermal, nanoassemble and electronic properties were also discussed. Meanwhile, the effect of the water-soluble FNPs on scavenging of free radicals was investigated in vitro as well. Furthermore, maybe as a nanoantioxidant, it enhanced the drought tolerance of

maize. In particular, it was preliminarily found that the maize germination was promoted by the newly synthesized FNPs.

Experimental procedure

Materials and equipment

All chemicals, unless otherwise stated, were purchased from commercial sources and used without further purification. C_{60} (purity >99.9%) was purchased from Henan Puyang Yongxin Reagents Company (China). 1,1-Diphenyl-2-picrylhydrazyl radical (DPPH·), 2,2′-azino-bis(3-ethylbenzo-thiazoline-6-sulfonic acid diammonium salt) (ABTS) and potassium persulfate ($K_2S_2O_8$) were purchased from Sigma-Aldrich (Shanghai) Trading Company (China). All of the other reagents and solvents were at least analytical grade.

The product was analyzed with matrix-assisted laser desorption ionization time-of-flight mass spectrometry (MALDI-TOF-MS, Autoflex, Bruker, Germany). The high-resolution ^{1}H nuclear magnetic resonance spectra were recorded in Fourier transform mode at 22 °C on a Bruker AVANCE 500 spectrometer (^{1}H–NMR, Bruker, Germany). Fourier transform infrared spectra were performed on a Thermo Scientific Nicolet iN10 MX spectrometer (FTIR, Madison, USA). UV-Visible absorption spectra under ambient temperature were recorded on a Shimadzu UV-2550 spectrophotometer (UV-Vis, Shimadzu, Japan). The absorbances were recorded on a Unico 2100 spectrophotometer (Shanghai Instruments, China). Thermogravimetric analysis (TGA) and differential scanning calorimetry (DSC) were performed on a NETZSCH STA 449C Thermogravimetric Analyzer (TA Instruments, Germany) attached to a model 2910 DSC cell, at a heating rate of 10 °C/min under nitrogen (N_2) atmosphere, in a scanning range from 45 to 800 °C. The average hydrodynamic diameter (HD), particle size distribution, and polydispersity index of the product were measured using a NanoBrook Omni particle size and zeta potential analyzer (Brookhaven Instruments, USA). The scanning electron microscopy images were photographed by a Hitachi S-4800 field-emission microscope (SEM, Hitachi, Japan). All electron spin resonance (ESR) experiments were carried out by using a JES-FA200 X-band ESR spectrometer (JEOL, Japan). The powder and aqueous solution of the sample were placed in the thin sealed glass capillary (0.5 mm).

Large-scale preparation of fullerenols

The water-soluble fullerenols was synthesized under O_2/NaOH condition with some modification (Husebo et al. 2004; Xing et al. 2004). Briefly, 400 mL 0.1 g/mL (equal to 2.5 mol/L) NaOH was mixed with 400 mL *o*-dichlorobenzene (ODCB) solution containing 10.8 g pristine fullerene C_{60} in a 2000 mL volume of beaker, and then 1.0 mL 40% TBAH were added as phase-transfer catalyst. The mixture was vigorously stirred by a mechanical agitator at room temperature under air. For 24 h, when the deep purple ODCB layer on the understratum of the reaction system became colorless, while the aqueous layer on the superstratum was changed from the originally colorless to deep brown, the ODCB layer was separated and washed twice with deionized water. The combined aqueous solution was filtered, followed by dialysis against deionized water using a dialysis membrane with molecular weight cutoff of 3500 Da until the pH of effluent was consistent. The dialysate was filtered through a 0.45-μm filter membrane, concentrated and dried on a rotary evaporator at 60 °C. Finally, the purified powder was obtained and marked as **FoI**, whereafter identified as $[C_{60}(OH)_{22}{\cdot}8H_2O]_n$; yield 17.47 g, 94.1%.

$ABTS^{+\cdot}$ scavenging assay

The scavenging activity to $ABTS^{+\cdot}$ radicals were measured, following the method in the literatures with slight modification (Li et al. 2012b; Wang et al. 2011). Briefly, $ABTS^{+\cdot}$ was produced by mixing 20 mmol/L phosphate buffer solution of 7.4 mmol/L 4.0 mL ABTS and 2.6 mmol/L 4.0 mL $K_2S_2O_8$. The mixture was kept in the dark at room temperature for 12 h to allow completion of radical generation, followed by dilution with phosphate buffer solution so that the absorbance of the stock $ABTS^{+\cdot}$ at 734 nm was 1.32 ± 0.02. Then, 1.5 mL diluted $ABTS^{+\cdot}$ solution was mixed into 3 mL by diluting the phosphate buffer solution of **FoI**, which the concentrations varied between 12.5 and 225 μg/mL. The UV-Vis spectra and the absorbances at 734 nm were recorded at 6 min after addition of **FoI**. The inhibition percentage of the samples was calculated using Eq. (1):

$$\text{Inhibition}\% = \frac{A_0 - A}{A_0} \times 100\% \quad (1)$$

where A_0 and A are the absorbances of $ABTS^{+\cdot}$ at 734 nm before and after infusion of **Fol** for each treatment, respectively.

DPPH· scavenging assay

The scavenging activity to DPPH· was determined, following the method in the literature (Li et al. 2012b). Briefly, 11 samples were prepared that 1.5 mL of the stock ethanol-water (v/v = 20:80) binary solution of DPPH· (110 μg/mL) were mixed into 3 mL using the binary solution of **Fol** with the concentrations between 10 and 383 μg/mL. The absorbances at 519 nm were recorded at 30 min after addition of **Fol**. The inhibition percentage of the samples was calculated with Eq. (1). The absorbance of **Fol** at 519 nm must be deducted.

Maize treatments

Mature maize (*Zea mays* L. cv. Zhengdan 958) seeds were selected and sterilized as described in our previous work (Wang et al. 2014). All seeds were washed thoroughly and soaked with water, 5 and 50 μg/mL of **Fol**, respectively. The seeds were placed in culture dish with water, 5 and 50 μg/mL of **Fol** incubated at 25 °C for germination 20 h after inhibition, respectively. The germination of seed samples was analyzed as follows: seed germination energy (%) = the number of germinated seeds on 2 days × 100 / the number of original seeds; seed germination rate (%) = the number of germinated seeds on 4 days × 100 / the number of original seeds; seed germination index (GI) = $\sum(Gt/Dt)$, where Gt is the germination rate at different days and Dt is the time in days. The germinated seeds were taken photos at 4 days after germination.

After germination, the maize seedlings were cultured with water, 5 and 50 μg/mL of **Fol** in a light chamber (day 28 °C/night 22 °C, relative humidity 75%) with a 16/8 h day/night cycle, respectively. When the second leaves were fully expanded, the seedlings were exposed to 15% PEG (MW6000) solution. The leaves were sampled for physiological parameters analysis at 2, 10, 24, or 48 h after treatment.

Contents of MDA and H_2O_2 and antioxidant enzyme assay

The activity of catalase (CAT) and superoxide dismutase (SOD) and the content of malondialdehyde (MDA) were measured with the corresponding kids according to the manufacturer's specifications (Jiangcheng, China). Leaf samples (0.1 g) were homogenized with a mortar and pestle at 4 °C in 0.9 ml normal saline to examine the activity of CAT and the content of MDA and H_2O_2. The homogenates were centrifuged according to the instructions. For SOD activity, leaf samples (0.25 g) were homogenized with a mortar and pestle at 4 °C in 1.0 ml normal saline. The homogenates were centrifuged at 3500 rpm for 10 min. The supernatants were measured by a spectrophotometer. Finally, the corresponding contents of MDA and H_2O_2 and antioxidant enzyme activities were analyzed according to the instructions.

Statistical analysis

Each physiology and radical scavenging experiment was at least triplicate. Data were expressed as means ± standard error (SE). All mean comparisons were done using the Student's t test for independent samples. In all cases, the confidence coefficient was set at 0.05.

Results and discussions

General approach for facile and scalable fabrication of FNPs

Our engineering aimed to produce FNPs with large-scale productivity. The general approach for one-step preparation of the water-soluble FNPs under improved O_2/NaOH condition is depicted in Fig. 1, which

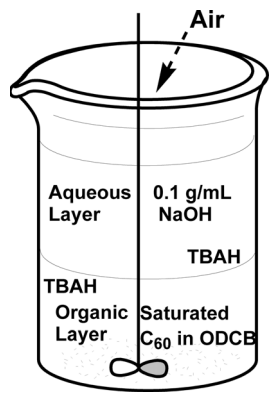

Fig. 1 General approach for one-step fabrication of water-soluble $C_{60}(OH)_{22}\cdot 8H_2O$ with large-scale productivity by improved alkaline-oxidation approach

fabrication up to 10 g was performed in laboratory and could also be directly used in industrial production if needed. Previously, no one considered that extremely concentrated NaOH (e.g., 1.0 g/mL) solution was strong corrosion and unnecessary as the hydroxylation reagent. The low-volume concentrate of NaOH led to form bulk quantities of sludge at the onset of the hydroxylation step, which O_2 in air was hard to further attack the sludgy intermediates on the bottom of the reaction container and subsequently resulted in unacceptable water-insoluble by-product. Furthermore, a huge volume of the solvents with low dissolving capacity were utilized without regard to high pollution, barrier to bulk production and economizing through the elimination of the normally high volumes. Herein, our group selected the moderately concentrated NaOH (e.g., 0.1 g/mL) solution as the hydroxylation reagent and ODCB (the value of C_{60} was 27 mg/mL under room temperature (Beeby et al. 1994)) as the best solvent after tens of experiments. In comparison with the approaches in the literatures (Alves et al. 2006; Husebo et al. 2004; Li et al. 1993), the innovation of our engineering is significance that the feed concentration of the hydroxylation reagent cut down to one tenth and the volume of the solvent decrease at least by 90% at an equal productivity of FNPs. Significantly, the hydrophilic intermediates from the hydroxylation step (Wang et al. 2015a) were quickly coming close to the aqueous NaOH layer on the upper of the reaction system with the H_2O-ODCB binary solvents and had plenty of opportunity exposure to O_2 originated from air, attacked easily by O_2, followed closely by conversion into the water-soluble product after exhaustive rehydroxylation and structural rearrangement, due to the availability of a large volume of mildly concentrated NaOH solution as the hydroxylation reagent and ODCB as solvent. Almost no sludge or precipitate was detected in this innovative process. After reaction, the raw product was separated from ODCB phase and filtered, and the final product of the water-soluble FNPs (abbreviated as **FoI**) was dried and then obtained after dialysis, to avoid the repeated precipitation with vast methanol, for a complete removal of TBAH and NaOH.

Our one-step strategy for the fabrication of **FoI** by improved O_2/NaOH approach is promising with considerable merits: (1) the reaction can be performed with a minimum of solvent under relatively mild alkaline condition; (2) the hydroxylation and oxidation processes are synergistic and easily manageable; (3) the after-treatment is labor-saving and simple; (4) almost no water-insoluble by-product is formed; (5) the product have almost no other groups (e.g., carbonyl, hereinafter proved by FTIR) except the desired -OH is anchored on the pristine fullerenes; and (6) the engineering leads to a weight increase of the product compared with the pristine fullerenes and increase of productivity.

Characterization

The structure of **FoI** was characterized by a variety of spectroscopic techniques. Figure 2a was the positive-ion mode MALDI-TOF-MS for **FoI** in deionized water, obtained using dithranol as matrix, which had only a single prominent ion peak at *m/z* 720. The isotope profile was expanded views at around *m/z* 720 and was conformable with those calculated from natural isotopic abundance, which was attributed to isotopic variants of $C_{60}^{+\cdot}$ (Jagerovic et al. 1996). It provided the convincing evidence that **FoI** was the derivative of fullerene C_{60}. In the ^{1}H-NMR spectrum of **FoI** shown in Fig. 2b, singlet resonance peak corresponding to the protons of -OH was observed at 4.8 ppm. The results of TOF-MS and ^{1}H-NMR are consistent with what have been observed for other FNPs (Yao et al. 2010). The FTIR spectrum of **FoI** is depicted in Fig. 2c and showed characteristic features at 1060, 1370, 1587, and 3397 cm^{-1}, which were assigned to νC-OH, δ_SC-OH, νC=C, and νO-H adsorptions. These characteristics of signals were reported for ever as diagnostic criteria for various FNPs (Chiang et al. 1992b; Husebo et al. 2004; Kokubo et al. 2008; Kokubo et al. 2011; Li et al. 1993; Schneider et al. 1994; Vileno et al. 2006; Xing et al. 2004), which elucidated the existence of -OH and of the remaining π-bonded carbons of the C_{60} cage in **FoI**. It was noteworthy that **FoI** had no the absorption peak between 1587 and 1800 cm^{-1}, which implied the non-existence of the impure oxygenous groups such as carboxylic group O-C=O, carbonyl group C=O, and hemiacetal structure (Chiang et al. 1992b; Kokubo et al. 2008; Kokubo et al. 2011; Li et al. 1993; Schneider et al. 1994; Xing et al. 2004). Combined with the MS result, the FTIR result revealed that the molecular structure of **FoI** was much more stable than those of FNPs reported by Xing et al. (2004), which the impure groups led to a cage-opened structure and lower the stability of FNPs. As shown in Fig. 2d, UV-Vis absorption spectrum of aqueous solution of **FoI** exhibited a broad

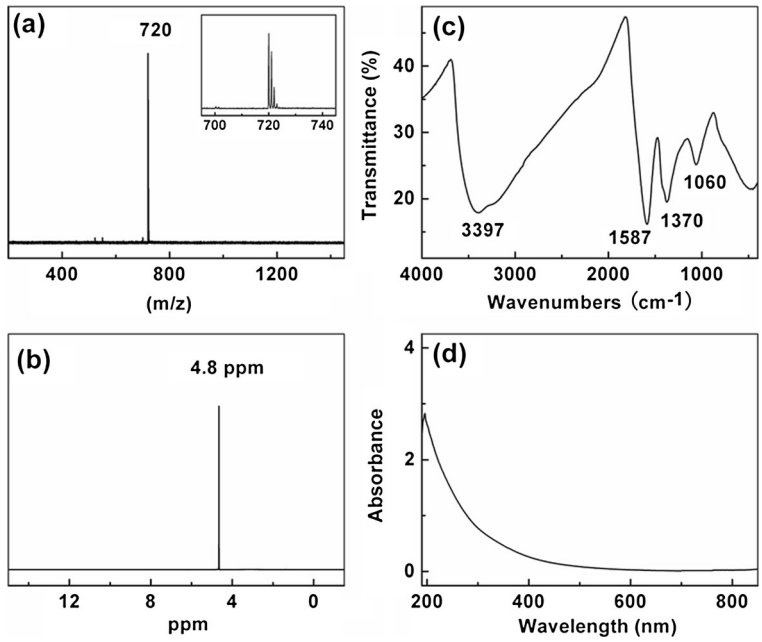

Fig. 2 MALDI-TOF-MS (**a**), ^{1}H-NMR (**b**), FTIR (**c**), and UV-Vis spectra (**d**) of $C_{60}(OH)_{22}\cdot 8H_2O$

asymmetrical decrease in absorbance with the wavelength range of 200 to 900 nm. The spectrum, no visible absorption zones, was featureless, in which similar results were obtained for FNPs synthesized by the variable methods (Kokubo et al. 2008; Vileno et al. 2006).

Thermal analysis

The TGA and DSC measurements were used to evaluate the decomposition behaviors of **FoI** and also to evaluate the -OH number attached to its carbon cage. The TG, differential thermogravimetry (DTG), and DSC thermograms under N_2 atmosphere are shown in Fig. 3. It revealed two-step degradation at "lower" range of temperatures (ca. 45–208 °C) and complex multistep

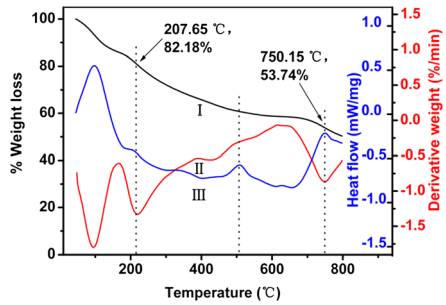

Fig. 3 Derivatograms of $C_{60}(OH)_{22}\cdot 8H_2O$ obtained under N_2 atmosphere at a 10 °C/min heating rate: *I*, TG curve; *II*, DTG curve; *III*, DSC curve

decomposition at "higher" range of temperatures (ca. 208–750 °C). At "lower" range of temperatures, the percentage weight loss of **FoI** to the extent of 6.35% occurred between 45 and 95 °C in the first step, which the initial weight loss could be negligible due to the removal of low boiling units or volatiles according to the literature (Cataldo et al. 2008b). The second-step decomposition of **FoI** was due to weight loss (11.47%) of second bound water from 95 to 208 °C. The water molecules entrapped tightly in fullerenols could not be dissociated by the usual heating up to 150 °C (Chiang et al. 1993; Kokubo et al. 2008). It was also supported by a small DSC endotherm at 180 °C and a strong DTG peak. From DTG curve, the onset thermal decomposition began at 95 °C and the bound water was completely removed up to 208 °C, which the maximum decomposition temperature (crest temperature) was obtained at 165 °C.

At "higher" range of temperatures, the release mass of **FoI** was assigned to the process of dehydroxylation, which had been usually interpreted in terms of eliminating all of -OH as reported for other fullerenols such as $C_{60}(OH)_{28}$ (Singh and Goswami 2011), $C_{60}(OH)_{36}\cdot 8H_2O$ (Kokubo et al. 2008), and $C_{60}(OH)_{40}\cdot 9H_2O$ (Kokubo et al. 2008). Five small endothermic peaks at 295, 393, 460, 610, and 655 °C were shown in the DSC thermogram, which the dehydroxylated process of **FoI** experienced clearly to

the distinct stepwise degradation. It was associated with these observations in the DTG curve. **Fol** was decomposed steady and continuously from 208 to 630 °C in the TG curve, and then, the weight loss exhibited a significant staged decrease up to 750 °C. TG trace showed a weight loss to the extent of 28.44% from 208 to 750 °C. In addition, it is noteworthy that a sharp and relatively weak exotherm with crest temperature at around 510 °C was observed by DSC. This makes an agreement with those found for fullerene-amine adduct (Janaki et al. 2000). It may be attributed to some structural rearrangement and/or relaxation process associated with elimination by cleaving the segmental appendant groups (Cataldo et al. 2008a; Janaki et al. 2000).

Thermal analysis techniques have been successfully exploited to calculate the -OH number in fullerenols, which is denoted in Eq. (2) (Goswami et al. 2004; Singh and Goswami 2011).

$$x = \frac{720}{M_1} \times \frac{y_1}{y_2} \quad (2)$$

where M_1 is the weight of each appendant -OH and equals to 17. y_1 is the percentage weight loss corresponded to the removal of all of -OH per fullerene cage. y_2 is the percentage weight loss plus char residue due to fullerene C_{60} only. Turning back to Fig. 3, the summary of the detailed and critical data reproduced in Table 1, sum of x have been calculated to be 22.4 for **Fol** based on the simultaneous TG-DTG-DSC analysis. Taking into account that molecule cannot be fractioned (Singh and Goswami 2011), thus **Fol** was described as the average molecular formula $C_{60}(OH)_{22}$. Moreover, to further validate the number of bound water (denoted as m) in **Fol**, the authors proposed the following formula (Eq. (3)) to calculate the value of m.

$$m = \frac{720}{M_2} \times \frac{y_3}{y_2} \quad (3)$$

where M_2 (equal to 18) is the weight of each water molecule. y_3 is the percentage weight loss corresponded to the removal of all bound water per fullerene cage. Sum of m have been calculated to be 8.48 for **Fol**, which was further expressed as $C_{60}(OH)_{22}\cdot 8H_2O$.

Size distribution and morphology of nanoassembly $[C_{60}(OH)_{22}\cdot 8H_2O]_n$

$C_{60}(OH)_{22}\cdot 8H_2O$ (50 μg/mL) in deionized water were successively measured 30 times by dynamic light scattering (DLS) technique with a NanoBrook Omni particle size and zeta potential analyzer, and one outlier was discarded. As shown on Fig. 4, $C_{60}(OH)_{22}\cdot 8H_2O$ formed aggregates and displayed monomodal nanosized distributions, the mean HD and polydispersity index were 138.1 ± 3.2 nm and 0.35, respectively. These results indicated that $C_{60}(OH)_{22}\cdot 8H_2O$ had a strong tendency to nanoassembly in water. Figure 5 shows the surface morphologies of the aggregates by SEM, which one drop of the aqueous solution (50 μg/mL) was deposited onto the silicon wafer substrate, followed by drying in air, finally coating with gold. The representative SEM images shown in Fig. 5a, b presented the nanoscale particle-aggregated structure of $C_{60}(OH)_{22}\cdot 8H_2O$. Thus, **Fol** nanoparticles could be described as $[C_{60}(OH)_{22}\cdot 8H_2O]_n$. As shown in Fig. 5c, d, the microstructure of $[C_{60}(OH)_{22}\cdot 8H_2O]_n$ were exhibited at higher magnification and were irregular near-spheres with smooth surface. The sizes of 60 granules of $[C_{60}(OH)_{22}\cdot 8H_2O]_n$ (in Fig. 5c) were statistically analyzed with a formal randomization procedure. The average size was 122.3 ± 2.2 nm with distribution in the range of 85–150 nm. It was in agreement with the conclusion by DLS analysis.

ESR measurements of $[C_{60}(OH)_{22}\cdot 8H_2O]_n$

he ESR spectra of $[C_{60}(OH)_{22}\cdot 8H_2O]_n$ in solid state and in aqueous solution were measured at 22 °C by a

Table 1 Calculation of the number of -OH and bound water per fullerene for **Fol** on the basis of TGA and DSC results

Code	% Weight loss (temperature range °C)				M_1	$x = \frac{720*y_1}{M_1*y_2}$	M_2	$m = \frac{720*y_3}{M_2*y_2}$
	Loss due to volatiles	y_3 (loss due to bound water)	y_1	y_2				
Fol	6.35 (45–95)	11.47 (95–208)	28.44 (208–750)	53.74 (> 750)	17	22.41	18	8.48

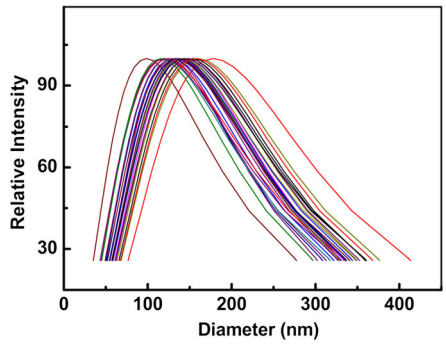

Fig. 4 Size distribution of 50 μg/mL $[C_{60}(OH)_{22}\cdot 8H_2O]_n$ aggregation in deionized water obtained by DLS, showing an average HD of 138.1 ± 3.2 nm, successively measured 30 times and discarded one outlier

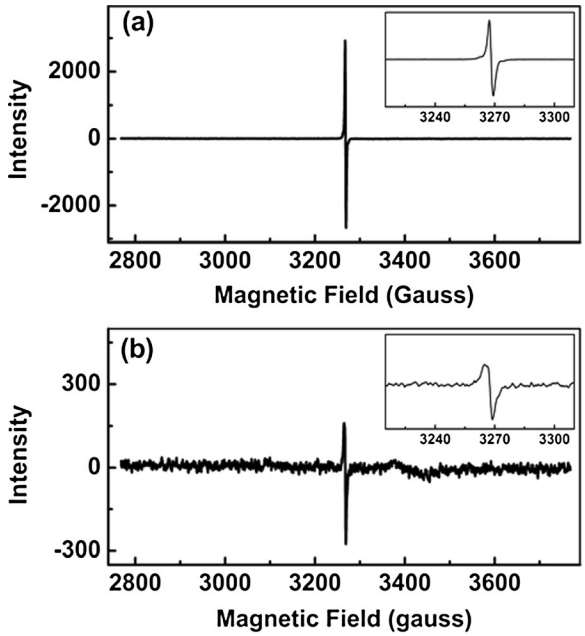

Fig. 6 ESR spectra for $[C_{60}(OH)_{22}\cdot 8H_2O]_n$ in solid-state (**a**) and in deionized water (**b**) obtained on a conventional X-band spectrometer at 22 °C. The *insets* are the region of magnetic field 3215–3310 G

conventional X-band spectrometer and shown in Fig. 6a, b, respectively. The silimar spectral patterns were observed but the relative intensity and resolution of the peaks differed significantly. The powder sample yielded an intense and sharp ESR signal at around 3268.2 G and corresponded to $g = 2.00001$ and $S = 1/2$, which was in good agreement with the results of $Na_n^+[C_{60}O_x(OH)_y]^{n-}$ n = 2–3, x = 7–9, y = 12–15 at 1.5 K ($g = 2$, $S = 1/2$) reported by Husebo et al. (2004). This signal shown in the inset of Fig. 6a for the expanded region of magnetic field from 3215 to 3310 G was no hyperfine structure. The g value and paramagnetic $S = 1/2$ spin state revealed that an odd number of electrons existed on $C_{60}(OH)_{22}\cdot 8H_2O$ fullerenol core. It indicated that the newly synthesized $[C_{60}(OH)_{22}\cdot 8H_2O]_n$ was a stable radical such as cyclopentadienyl radicals and could be used as a spin-trapping agent to eliminate free radicals (Husebo et al. 2004).

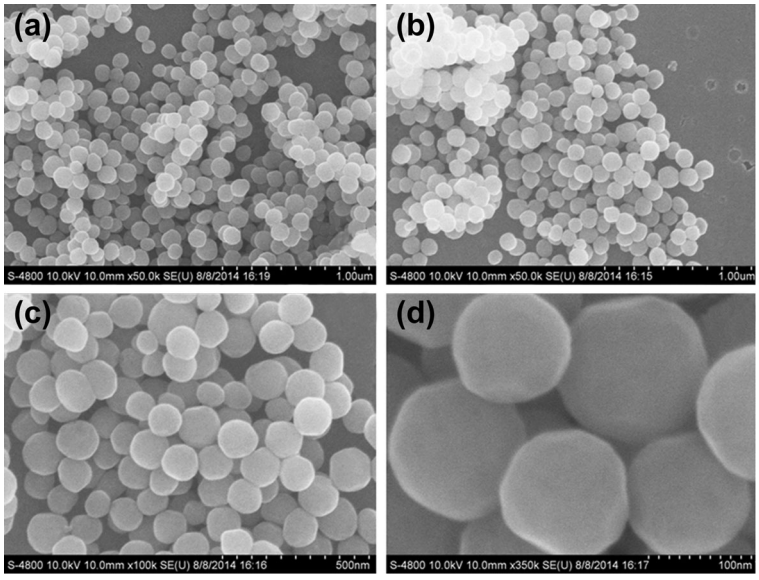

Fig. 5 Representative SEM images of $[C_{60}(OH)_{22}\cdot 8H_2O]_n$ (**a**) × 50,000, (**b**) × 50,000, (**c**) × 100,000, (**d**) × 350,000. Those of **c** and **d** are the local zoom within the area of **b**

In vitro scavenging activity of free radicals by $[C_{60}(OH)_{22}\cdot 8H_2O]_n$

To investigate whether or not $[C_{60}(OH)_{22}\cdot 8H_2O]_n$ can scavenge free radicals in vitro, experiments were performed using the nitrogen-centered radicals $ABTS^{+\cdot}$ and DPPH· and determined by spectrophotometry, which their structures were shown in the inset of Figs. 7b and 8, respectively. The effects of $[C_{60}(OH)_{22}\cdot 8H_2O]_n$ on the UV-Vis spectra of $ABTS^{+\cdot}$ radicals are depicted in Fig. 7a. A gradual reduction of the intensity of the absorbance peak at 734 nm was associated to the addition of $[C_{60}(OH)_{22}\cdot 8H_2O]_n$ with concentrations from 12.5 to 225 μg/mL, which illustrated that contents of $ABTS^{+\cdot}$ were reduced. In other words, $[C_{60}(OH)_{22}\cdot 8H_2O]_n$ can scavenge $ABTS^{+\cdot}$ radicals in vitro in a dose-dependent manner. Figure 7b shows the correlations between the clearance and the contents of $[C_{60}(OH)_{22}\cdot 8H_2O]_n$. The inhibition percentage of $ABTS^{+\cdot}$ radicals was suddenly increased from 17.2 to 96.2% when $[C_{60}OH)_{22}\cdot 8H_2O]_n$ was added with concentration from 12.5 to 150 μg/mL, and then reached to 96.8% until up to 225 μg/mL. The change of the inhibition percentage correlated to the concentrations was fitted by a three-parameter single exponential function of the nonlinear curve analysis with Origin 7.5 professional software. IC_{50} value of $[C_{60}(OH)_{22}\cdot 8H_2O]_n$, defined as the concentration of 50% inhibition percentage (Li et al. 2012b), was calculated to 45.3 ± 0.6 μg/mL. In addition, the change of the inhibition percentage of DPPH· radicals with concentration were plotted in Fig. 8, showed gradual increase from 2.5 to 24.6% after injection of $[C_{60}(OH)_{22}\cdot 8H_2O]_n$ with concentration from 10 to 128 μg/mL. Maximal inhibition percentage of DPPH· (30.4%) was found at around 160 μg/mL, followed by slight decrease (26.5% at 223 μg/mL and 22.8% at 383 μg/mL). It has been reported that DPPH· and $ABTS^{+\cdot}$ may be scavenged via donation of hydrogen atom (H·) to from a stable DPPH-H molecule (Li et al. 2012b) and via an electron (e) transfer reaction (Li et al. 2012b; Prior and Cao 1999), respectively. The scavenging effect of $ABTS^{+\cdot}$ is significantly higher than that of DPPH· by $[C_{60}(OH)_{22}\cdot 8H_2O]_n$. It suggested that $[C_{60}(OH)_{22}\cdot 8H_2O]_n$ more easily exerted radical scavenging action via donating electron (e) than donating H·. Based on the discussion above, it revealed that $[C_{60}(OH)_{22}\cdot 8H_2O]_n$ will be an ideal candidate as a novel fullerene-based free radical scavenger in biological systems.

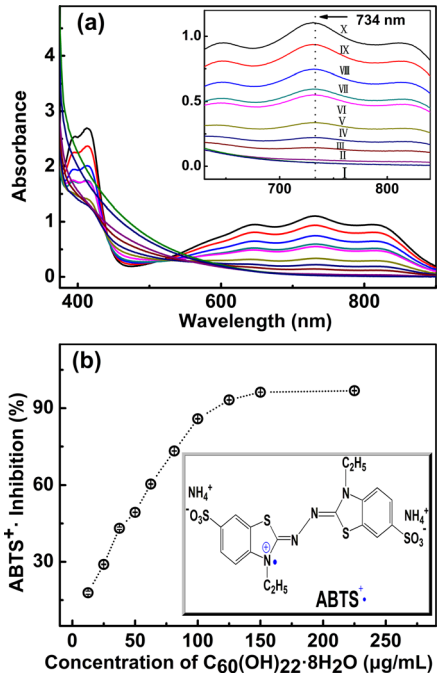

Fig. 7 UV-Vis spectra (**a**) and the percentage inhibition (**b**) of $ABTS^{+\cdot}$ treated by $[C_{60}(OH)_{22}\cdot 8H_2O]_n$ with concentrations increased from 12.5 (*I*) to 225 μg/mL (*X*). Data are mean values ± SE for triplicate. The *inset* of **a** and **b** are the region of wavelength from 630 to 840 nm and the structural formula of $ABTS^{+\cdot}$, respectively

Maize seeds germination promoted by $[C_{60}(OH)_{22}\cdot 8H_2O]_n$

Recently, various CNMs, including SWCNTs/MWCNTs, fullerenes and its derivates, have gained a lot of attentions on their potential applications in plant growth regulation (Khot et al. 2012; Mukherjee et al. 2016). In order to investigate the role in regulating plant growth of $[C_{60}(OH)_{22}\cdot 8H_2O]_n$, the germination of maize

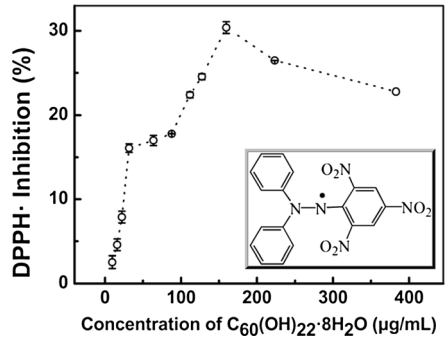

Fig. 8 The percentage inhibition of DPPH· treated by $[C_{60}(OH)_{22}\cdot 8H_2O]_n$ with concentrations increased from 10 to 383 μg/mL. Data are mean values ± SE for triplicate. The *inset* is the structural formula of DPPH·

Table 2 Effects of 0, 5 and 50 μg/ml $[C_{60}(OH)_{22}\cdot 8H_2O]_n$ on maize germination

Code	% Germination rate	% Germination force	Germination index
0 μg/ml	76.67 ± 0.96b	72.78 ± 1.47b	69.06 ± 0.37b
5 μg/ml	76.11 ± 0.56b	70.55 ± 1.47b	72.61 ± 1.13b
50 μg/ml	90.56 ± 1.11a	87.78 ± 1.11a	95.97 ± 1.35a

Data are mean values ± SE of three independent experiments. Within each set of experiments, different letters are significantly different at the 0.05 level

seeds soaked and cultured with $[C_{60}(OH)_{22}\cdot 8H_2O]_n$ were studied. As shown in Table 2 and in Fig. 9a, there was little or no effect on the germination of seeds treatment with 5 μg/mL $[C_{60}(OH)_{22}\cdot 8H_2O]_n$ solution compared with control. However, the germination rate, germination energy, and germination index of seeds were significantly enhanced by 50 μg/mL $[C_{60}(OH)_{22}\cdot 8H_2O]_n$. For example, the germination rate of seeds treatment with 50 μg/mL $[C_{60}(OH)_{22}\cdot 8H_2O]_n$ solution at 2 days postexposure were 65% while 40% for control. The results revealed that the concentration of FNPs played an important role in seed germination, but the effectiveness varied in different plant species (Lahiani et al. 2015). As shown in Fig. 9b, the shoots and roots of seedlings cultured in 50 μg/mL $[C_{60}(OH)_{22}\cdot 8H_2O]_n$ solution grew better than that of the control, and further studies found that the fresh weight was also obviously increased (data not shown). These findings were in an agreement with the previous reports, which FNPs enhanced bitter melon growth and

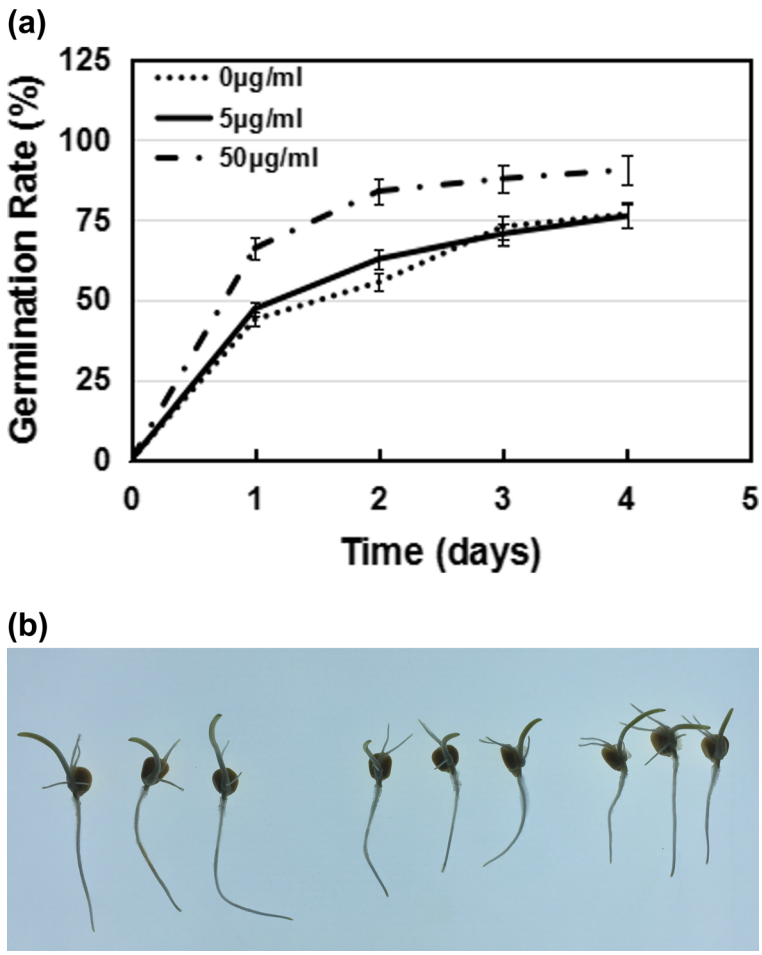

Fig. 9 Effects of 0, 5, and 50 μg/ml $[C_{60}(OH)_{22}\cdot 8H_2O]_n$ on seed germination of maize. **a** Time dependence of the germination rate. **b** The photograph of the seedlings at 4 days after germination; *left*, 50 μg/ml; *middle*, 5 μg/ml; *right*, 0 μg/ml. Data are mean values ± SE for triplicate

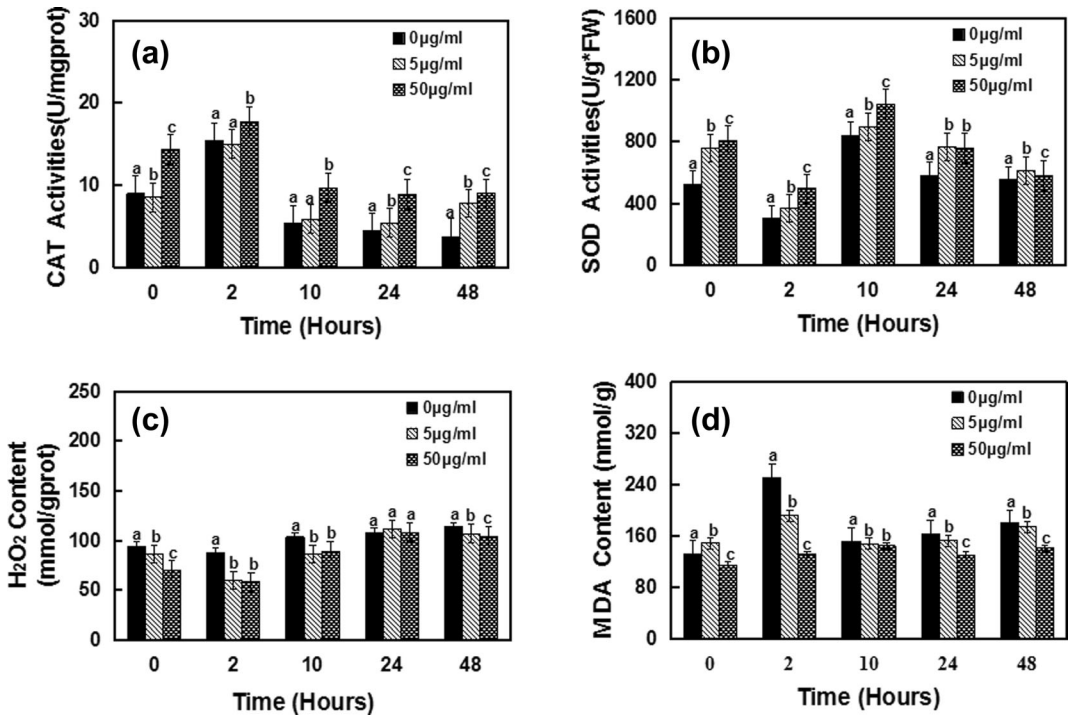

Fig. 10 Effects of 0, 5, and 50 μg/ml $[C_{60}(OH)_{22}{\cdot}8H_2O]_n$ on CAT (**a**) and SOD (**b**) activities, H_2O_2 (**c**) and MDA (**d**) contents in maize. Data are mean values ± SE for triplicate. Within each set of experiments, *bars with different letters* were significantly different at the 0.05 level

Arabdopsis hypocotyls length (Gao et al. 2011; Kole et al. 2013). These results suggested that $[C_{60}(OH)_{22}{\cdot}8H_2O]_n$ as a plant growth regulator has great potential applications in agriculture.

Maize seedlings tolerance to drought stress enhanced by $[C_{60}(OH)_{22}{\cdot}8H_2O]_n$

Some exogenous antioxidant substances (e.g., vitamin C as free radical scavenger) mediated plant tolerance to stress (Shalata and Neumann 2001; Xue et al. 2009). Turning back to Figs. 7 and 8, $[C_{60}(OH)_{22}{\cdot}8H_2O]_n$ could significantly scavenge $ABTS^{+\cdot}$ and DPPH· free radicals in vitro. Based on previous reports and our results, we speculated that $[C_{60}(OH)_{22}{\cdot}8H_2O]_n$ were involved in stimulating plant tolerance to stress.

In order to prove the hypothesis, the physiological indexes, including the protective enzyme (antioxidant enzymes SOD and CAT) activities and the contents of MDA and H_2O_2 were measured in maize cultured with 0, 5, and 50 μg/mL $[C_{60}(OH)_{22}{\cdot}8H_2O]_n$ solution under drought stress simulated by PEG, respectively. As shown in Figs. 10a, b, the SOD and CAT activities in seedlings had improved by $[C_{60}(OH)_{22}{\cdot}8H_2O]_n$ compared with control. The content of H_2O_2, a form of ROS generated as a result of oxidative stress, was decreased in maize seedlings cultured with $[C_{60}(OH)_{22}{\cdot}8H_2O]_n$ (Fig. 10c). As an indicator of stress-induced cell damage, the accumulation of MDA reflected usually the level of lipid peroxidation and also indirectly reflected the extent of membrane injury (Mittler 2002). It was noteworthy that MDA accumulation was significantly suppressed by 5 and 50 μg/mL of $[C_{60}(OH)_{22}{\cdot}8H_2O]_n$ solution for the entire length of the study (Fig. 10d, $P < 0.05$). The results showed that exogenous $[C_{60}(OH)_{22}{\cdot}8H_2O]_n$ could decrease the stress-induced damages in maize and enhance the plant tolerance to drought stress. Maybe $[C_{60}(OH)_{22}{\cdot}8H_2O]_n$ as an antioxidant remove the excessive accumulation of ROS in maize under drought stress and/or partially inhibit the extent of membrane injury like vitamin C, which need to be researched (Shalata and Neumann 2001). The possible reason might be that the new FNPs, to protect and increase the activities of antioxidant enzymes, played a role indirectly in antioxidant and promoted maize stress tolerance. Further studies of maize

stress tolerance, enhanced by $[C_{60}(OH)_{22}\cdot 8H_2O]_n$ through whatever mechanism (the former and/or the latter), is necessary.

Conclusions

In conclusion, a facile one-step technology to fabricate water-soluble FNPs in large quantity was developed by improved alkaline-oxidation approach using a large volume of moderately concentrated NaOH solution as the hydroxylation agent and ODCB as the solvent. It provided an economic way for industrial scale bulk production and less chemically impure groups of FNPs. The strategy is feasible in operation, convenient in practice, labor-saving, and inexpensive in cost. The resulted product, $[C_{60}(OH)_{22}\cdot 8H_2O]_n$, were characterized by various measurements including MALDI-TOF-MS, ^{1}H-NMR, FTIR, UV-Vis, TGA, DSC, DLS, SEM, and ESR. $ABTS^{+\cdot}$ and DPPH· scavenging assay in vitro confirm the high efficiency of $[C_{60}(OH)_{22}\cdot 8H_2O]_n$ as a novel free radical scavenger. Additionally, $[C_{60}(OH)_{22}\cdot 8H_2O]_n$ as an excellent candidate CNMs has the potential to serve as the plant defense stimulation agent, paving the avenue to new applications in agri-nanotechnology.

Acknowledgments The authors are grateful to the financial supports of the Natural Science Foundation of China (21305027, 11405185), the Public Welfare (Agriculture) Research Project of China (201303030), and the Key Project of Henan Educational Committee of China (16A210007 and 14A180005).

References

Alves GC, Ladeira LO, Righi A, Krambrock K, Calado HD, Gil RPDF, Pinheiro MVB (2006) Synthesis of $C_{60}(OH)_{18\text{-}20}$ in aqueous alkaline solution under O_2-atmosphere. J Brazil Chem Soc 17:1186–1190

Arrais A, Diana E (2003) Highly water soluble C_{60} derivatives: a new synthesis. Fuller Nanotub Car N 11:35–46

Beeby A, Eastoe J, Heenan RK (1994) Solubilization of C60 in aqueous micellar solution. J Chem Soc Chem Comm :173–175

Cataldo F, Ursini O, Angelini G (2008a) Radiation-cured polyisoprene/C_{60} fullerene nanocomposite. Part 2: synthesis in decalin. Radiat Phys Chem 77:742–750

Cataldo F, Ursini O, Angelini G (2008b) Radiation-cured polyisoprene/C_{60} fullerene nanocomposite. Part 1: synthesis in hexane and in toluene. Radiat Phys Chem 77:734–741

Chen ZY, Ma LJ, Liu Y, Chen CY (2012) Applications of functionalized fullerenes in tumor theranostics. Theranostics 2: 238–250

Chiang LY, Bhonsle JB, Wang LY, Shu SF, Chang TM, Hwu JR (1996) Efficient one-flask synthesis of water-soluble [60]fullerenols. Tetrahedron 52:4963–4972

Chiang LY, Swirczewski JW, Hsu CS, Chowdhury SK, Cameron S, Creegan K (1992a) Multihydroxy Additions onto C60 Fullerene Molecules. J Chem Soc Chem Comm :1791–1793

Chiang LY, Upasani RB, Swirczewski JW (1992b) Versatile nitronium chemistry for C_{60} fullerene functionalization. J Am Chem Soc 114:10154–10157

Chiang LY, Upasani RB, Swirczewski JW, Soled S (1993) Evidence of Hemiketals incorporated in the structure of fullerols derived from aqueous acid chemistry. J Am Chem Soc 115:5453–5457

Chiang LY, Wang LY, Swirczewski JW, Soled S, Cameron S (1994) Efficient synthesis of polyhydroxylated fullerene derivatives via hydrolysis of Polycyclosulfated precursors. J Org Chem 59:3960–3968

Djordjevic A, Srdjenovic B, Seke M, Petrovic D, Injac R, Mrdjanovic J (2015) Review of synthesis and antioxidant potential of fullerenol nanoparticles. J Nanomater 2015: 567073

Gao J et al (2011) Polyhydroxy fullerenes (fullerols or fullerenols): beneficial effects on growth and lifespan in diverse biological models. PLoS One 6:e19976

Goswami TH, Singh R, Alam S, Mathur GN (2004) Thermal analysis: a unique method to estimate the number of substituents in fullerene derivatives. Thermochim Acta 419:97–104

Grebowski J, Kazmierska P, Krokosz A (2013) Fullerenols as a new therapeutic approach in nanomedicine. Biomed Res Int. doi:10.1155/2013/751913

Husebo LO, Sitharaman B, Furukawa K, Kato T, Wilson LJ (2004) Fullerenols revisited as stable radical anions. J Am Chem Soc 126:12055–12064

Jagerovic N, Elguero J, Aubagnac JL (1996) Reaction of 2-azidobenzothiazole and 1-azido-4-(3′, 5′-dimethyl-1′-pyrazolyl) tetrafluorobenzene with [60] fullerene and characterization of the adducts by fast-atom bombardment mass spectrometry. Tetrahedron 52:6733–6738

Janaki J, Premila M, Gopalan P, Sastry VS, Sundar CS (2000) Thermal stability of a fullerene-amine adduct. Thermochim Acta 356:109–116

Khot LR, Sankaran S, Maja JM, Ehsani R, Schuster EW (2012) Applications of nanomaterials in agricultural production and crop protection: a review. Crop Prot 35:64–70

Kokubo K, Matsubayashi K, Tategaki H, Takada H, Oshima T (2008) Facile synthesis of highly water-soluble fullerenes more than half-covered by hydroxyl groups. ACS Nano 2: 327–333

Kokubo K, Shirakawa S, Kobayashi N, Aoshima H, Oshima T (2011) Facile and scalable synthesis of a highly hydroxylated water-soluble fullerenol as a single nanoparticle. Nano Res 4: 204–215

Kole C et al (2013) Nanobiotechnology can boost crop production and quality: first evidence from increased plant biomass, fruit yield and phytomedicine content in bitter melon (*Momordica charantia*). BMC Biotechnol 13:37

Lahiani MH, Chen JH, Irin F, Puretzky AA, Green MJ, Khodakovskaya MV (2015) Interaction of carbon nanohorns with plants: uptake and biological effects. Carbon 81:607–619

Li J, Takeuchi A, Ozawa M, Li XH, Saigo K, Kitazawa K (1993) C60 fullerol formation catalyzed by quaternary ammonium hydroxides. J Chem Soc Chem Comm 23:1784–1785

Li J et al (2012a) Separation and purification of fullerenols for improved biocompatibility. Carbon 50:460–469

Li XC, Lin J, Gao YX, Han WJ, Chen DF (2012b) Antioxidant activity and mechanism of Rhizoma Cimicifugae. Chem Cent J 6:140

Markovic Z, Trajkovic V (2008) Biomedical potential of the reactive oxygen species generation and quenching by fullerenes (C_{60}). Biomaterials 29:3561–3573

Mirkov SM et al (2004) Nitric oxide-scavenging activity of polyhydroxylated fullerenol, $C_{60}(OH)_{24}$. Nitric Oxide 11: 201–207

Mittler R (2002) Oxidative stress, antioxidants and stress tolerance. Trends Plant Sci 7:405–410

Mukherjee A, Majumdar S, Servin AD, Pagano L, Dhankher OP, White JC (2016) Carbon nanomaterials in agriculture: a critical review. Front Plant Sci 7:172

Nielsen GD, Roursgaard M, Jensen KA, Poulsen SS, Larsen ST (2008) In vivo biology and toxicology of fullerenes and their derivatives. Basic Clin Pharmacol Toxicol 103:197–208

Prior RL, Cao GH (1999) In vivo total antioxidant capacity: comparison of different analytical methods. Free Radic Biol Med 27:1173–1181

Ratnikova OV et al (2004) The new method for the synthesis of fullerols based on radical reaction. Fuller Nanotub Car N 12: 155–158

Schneider NS, Darwish AD, Kroto HW, Taylor R, Walton DRM (1994) Formation of fullerols via hydroboration of fullerene C60. J Chem Soc Chem Comm 4:463–464

Shalata A, Neumann PM (2001) Exogenous ascorbic acid (vitamin C) increases resistance to salt stress and reduces lipid peroxidation. J Exp Bot 52:2207–2211

Singh R, Goswami T (2011) Understanding of thermo-gravimetric analysis to calculate number of addends in multifunctional hemiortho ester derivatives of fullerenol. Thermochim Acta 513:60–67

Vileno B, Marcoux PR, Lekka M, Sienkiewicz A, Feher T, Forro L (2006) Spectroscopic and photophysical properties of a highly derivatized C_{60} fullerol. Adv Funct Mater 16:120–128

Wang CT, Yuan ZH, Li SP, Wang W, Xue RL, Tai FJ (2014) Characterization of eight CBL genes expressions in maize early seeding development. Acta Physiol Plant 36:3307–3314

Wang FF, Li N, Tian D, Xia GF, Xiao N (2010) Efficient synthesis of fullerenol in anion form for the preparation of electrodeposited films. ACS Nano 4:5565–5572

Wang S, He P, Zhang JM, Jiang H, Zhu SZ (2005) Novel and efficient synthesis of water-soluble [60]fullerenol by solvent-free reaction. Synthetic Commun 35:1803–1808

Wang XZ, Li XC, Chen DF (2011) Evaluation of antioxidant activity of isoferulic acid in vitro. Nat Prod Commun 6: 1285–1288

Wang ZZ, Lu ZH, Zhao YL, Gao XF (2015a) Oxidation-induced water-solubilization and chemical functionalization of fullerenes C_{60}, $Gd@C_{60}$ and $Gd@C_{82}$: atomistic insights into the formation mechanisms and structures of fullerenols synthesized by different methods. Nanoscale 7:2914–2925

Wang ZZ, Wang SK, Lu ZH, Gao XF (2015b) Syntheses, structures and antioxidant activities of fullerenols: knowledge learned at the atomistic level. J Clust Sci 26:375–388

Xing GM et al (2004) Influences of structural properties on stability of fullerenols. J Phys Chem B 108:11473–11479

Xiong FX, Li J, Wang HZ, Xing GM, He R (2016) Evaluation of a series of different surface charged fullerenol nanoparticles as reactive oxygen species scavengers and potential cytoprotective agents. J Nanosci Nanotechno 16:7170–7174

Xue TT, Li XZ, Zhu W, Wu CA, Yang GD, Zheng CC (2009) Cotton metallothionein GhMT3a, a reactive oxygen species scavenger, increased tolerance against abiotic stress in transgenic tobacco and yeast. J Exp Bot 60:339–349

Yao L, Kang F, Peng QY, Yang XL (2010) An improved method for fullerol preparation based on dialysis. Chinese J Chem Eng 18:876–879

Zhang JM, Yang W, He P, Zhu SZ (2004) Efficient and convenient preparation of water-soluble fullerenol. Chinese J Chem 22: 1008–1011

Zhang P, Pan HL, Liu DF, Guo ZX, Zhang FS, Zhu DB (2003) Effective mechanochemical synthesis of [60]fullerols. Synthetic Commun 33:2469–2474